Characterization of Depth-Dependent Loss for Visible Light Propagation in Underwater Optical Wireless Links

Alessandro Ugolini, Federica Poli
Department of Engineering and Architecture
University of Parma, Parma, Italy
alessandro.ugolini@unipr.it, federica.poli@unipr.it

Daniele Croce, Stefano Mangione
Department of Engineering
University of Palermo, Palermo, Italy
daniele.croce@unipa.it, stefano.mangione.tlc@unipa.it

***Abstract*—We describe the propagation of visible light in underwater wireless communications, with particular attention to vertical links. We compute power losses suffered by signals considering depth-dependent absorption, scattering, as well as the contribution of bubbles, under realistic channel conditions. We show how to select the best visible light wavelength to be used in transmission according to the specific channel characteristics.**

***Index Terms*—UOWC, vertical link, water channel properties, bubbles**

I. Introduction

Underwater optical wireless communications (UOWC) are an increasingly interesting research area due to their applications in beyond 5G scenarios [1]. For this reason, the accurate study of channel models is of the utmost importance, to identify the best transceiver solutions and achieve a realistic performance evaluation of the proposed technologies.

Most channel models commonly presented in literature classify water based on its turbidity [2], hence deriving a simplified channel description. However, this sort of model does not take into consideration the variations of the water characteristics at different depths. Hence, while it can be suitable for horizontal links, it becomes highly inaccurate for vertical ones [3].

For this reason, in this paper, we study the behavior of a vertical underwater link when light in the visible range is transmitted, by computing the channel attenuation at different wavelengths. Depth-dependent effects are considered in order to develop a realistic and accurate model for light propagation in a vertical underwater channel. The role of absorption, scattering, and air bubbles in water is studied and the losses induced on visible light by the channel are computed. Different wavelengths are compared with the aim of identifying the best settings in different realistic channel conditions. Results show that blue, cyan and green present the lowest attenuation coefficient, while yellow light can represent an alternative to blue and green in the first tens of meters beneath the surface.

The paper is structured as follows. Section II describes the depth-dependent effects occurring in the communication channel, in Section III the total power losses due to the propagation in the vertical underwater environment are computed, and Section IV concludes the paper.

II. Channel Characterization

A. Chlorophyll Concentration

The depth-dependent chlorophyll concentration profile has been subject of accurate research due to its importance in different fields. Typically, the chlorophyll concentration is higher closer to the surface and tends to vanish for higher depth. The deep chlorophyll maximum (DCM) is a peak in chlorophyll concentration, which is typically between 15 and 120 m, depending on the surface concentration of chlorophyll and on the characteristics of the water [4].

The chlorophyll profile as a function of depth $C_{\mathrm{c}}(z)$ can be described as a Gaussian curve depending on five numerically determined parameters. In general, it can be expressed as

$$C_{\mathrm{c}}(z) = B_0 + Sz + \frac{h}{\sigma\sqrt{2\pi}} \exp\left[\frac{-(z-z_{\max})^2}{2\sigma^2}\right] \tag{1}$$

where B_0 is the background chlorophyll concentration on the surface, S is the vertical gradient of concentration, which is always negative due to the slow decrease of $C_{\mathrm{c}}(z)$ with depth, h is the total chlorophyll above the background levels, and $z_{\max}$ is the DCM depth. The standard deviation of the chlorophyll concentration, σ, is computed as

$$\sigma = \frac{h}{\sqrt{2\pi}[C_{\mathrm{c}}(z_{\max}) - B_0 - Sz_{\max}]}, \tag{2}$$

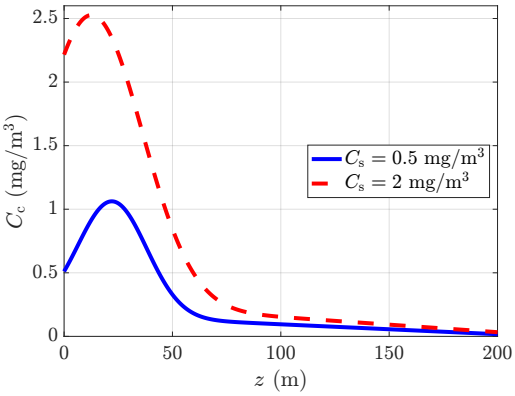

Fig. 1. Chlorophyll concentration versus depth for different values of the surface concentration C_{s}.

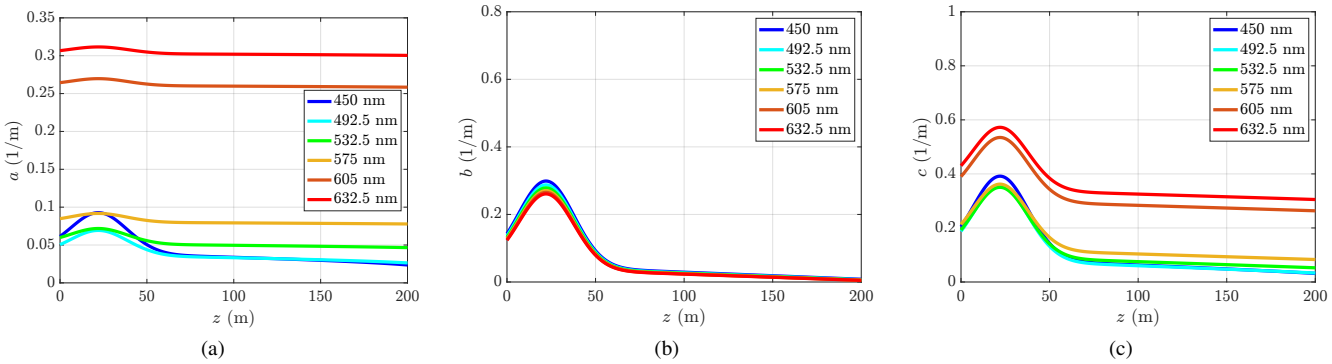

Fig. 2. Absorption (a), scattering (b), and overall attenuation coefficients (c) for surface concentration $C_{\mathrm{s}} = 0.5$ mg/m^3 and different signal wavelengths.

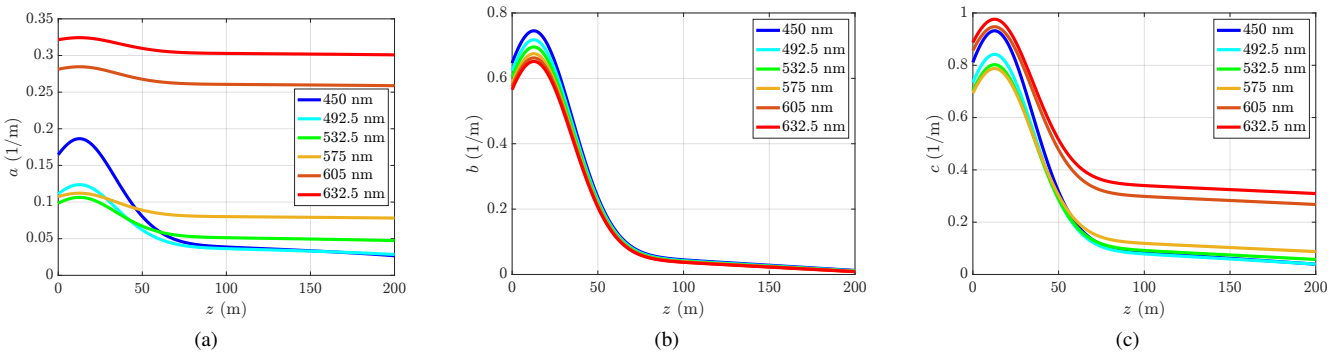

Fig. 3. Absorption (a), scattering (b), and overall attenuation coefficients (c) for surface concentration $C_{\mathrm{s}} = 2$ mg/m^3 and different signal wavelengths.

The parameters used in this paper in Eqs. (1) and (2) refer to the *cold water* case described in [4], and can be found in [4, Tab. 5].

The behavior described by Eq. (1) is represented in Fig. 1 for the two different values of the surface chlorophyll concentration C_{s} considered in this paper. Clearly, the higher the value of C_{s}, the higher the peak in the chlorophyll distribution. We also notice how the distribution of the chlorophyll tends to zero as the depth increases. The next section analyzes the impact of these aspects on the attenuation of visible light in water.

B. Absorption and Scattering

In general, the chlorophyll depth distribution affects the propagation of light in water. Its attenuation effect can be modeled by means of a wavelength-dependent attenuation coefficient $c(\lambda)$

$$c(\lambda) = a(\lambda) + b(\lambda)\,, \tag{3}$$

which is composed of two main contributions, attenuation, described by $a(\lambda)$, and scattering, represented by $b(\lambda)$, respectively. Many models in the literature assume that the water characteristics do not change with depth, i.e., the values of a and b (and hence of c) are constant with depth. This assumption is convenient to model horizontal, but it can lead to an incorrect analysis when vertical links are considered. In fact, both the absorption and scattering coefficients are depth-dependent, and Eq. (3) can be rewritten as

$$c(\lambda, z) = a(\lambda, z) + b(\lambda, z)\,. \tag{4}$$

A detailed description of the computation carried on using Eq. (4) taking into account the chlorophyll profile is reported in [5], while the parameters used to characterize the water as a function of both wavelength and depth can be found in [6]–[8].

Figs. 2 and 3 report the values of $a(\lambda, z)$, $b(\lambda, z)$, and $c(\lambda, z)$ for the two considered values of C_{s}, respectively, as a function of the depth z. The different colors correspond to possible wavelengths in the visible spectrum, related to feasible laser sources [9]–[11]. We notice that blue, cyan and green present the lowest attenuation coefficient, while orange and red are the most heavily impaired wavelengths. Notice that yellow light can represent an alternative to blue and green one in the first tens of meters beneath the surface, since it is more absorbed by water, but it is less affected by scattering. Moreover, as expected, higher C_{s} values cause significantly larger attenuation, for all wavelengths.

C. Air Bubbles in Water

Another important effect that can have a significant impact on the propagation of light in water is the presence of air bubbles in the first layers below the surface. Air bubbles are caused by wind and waves. In particular, a large bubble population is generated after the breaking of a wave. While

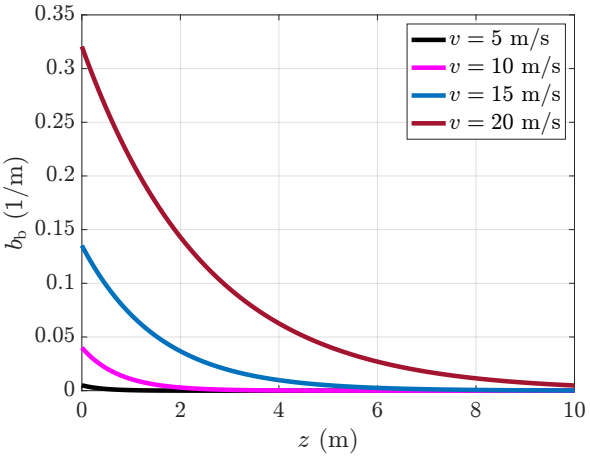

Fig. 4. Scattering coefficient due to bubbles for different wind speeds.

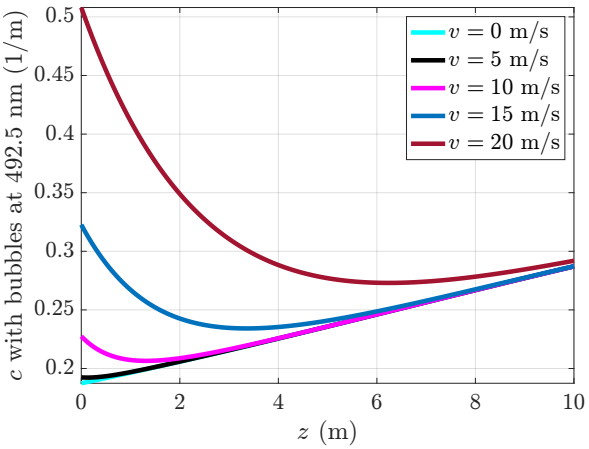

Fig. 5. Attenuation coefficient versus depth for surface concentration $C_\mathrm{s} = 0.5$ mg/m^3 and $\lambda = 492.5$ nm, including bubble contribution.

large bubbles dissolve rapidly, small ones may persist for a few tens of minutes after the wave has broken, thus affecting the light propagation by increasing the level of scattering [12].

The Hall-Novarini bubble population model is used to describe the radiative properties of bubbles as a function of depth and wind speed [12]. It can be shown that the bubble number density (in m^{-3}) as a function of the depth z can be approximated as

$$N(z) \simeq (1.6 \cdot 10^{10}) \frac{r_{\mathrm{ref}}^4(z)}{3 r_{\mathrm{min}}^3} \left(\frac{v_{10}}{13}\right)^3 \exp\left(-\frac{z}{L(v_{10})}\right), \quad (5)$$

where $r_{\mathrm{ref}}(z) = 54.4 \cdot 10^{-6} + 1.984 \cdot 10^{-6} z$ is the bubble reference radius, $r_{\mathrm{min}} = 10$ μm is the minimum bubble radius, v_{10} is the wind speed at 10 m above sea level (in m/s), and

$$L(v_{10}) = \begin{cases} 0.4 & \text{if } v_{10} < 7.5 \text{ m/s} \\ 0.4 + 0.115(v_{10} - 7.5) & \text{if } v_{10} \geq 7.5 \text{ m/s}. \end{cases} \quad (6)$$

Finally, the bubble dependent scattering coefficient can be computed as [12]

$$b_\mathrm{b}(z) = N(z) Q_{\mathrm{sca}} S_\mathrm{b}, \quad (7)$$

where Q_{sca} is the bubble mean scattering efficiency, equal to 2 for bubbles with radius greater than 1 μm, and $S_\mathrm{b} \simeq 3\pi r_{\mathrm{min}}^2$ is the bubble average geometric cross-sectional area. The coefficient $b_\mathrm{b}(z)$ is reported in Fig. 4 for different wind speed values.

Taking into consideration the effect of bubbles, the overall depth-dependent attenuation coefficient can be written as

$$c(\lambda, z) = a(\lambda, z) + b(\lambda, z) + b_\mathrm{b}(z). \quad (8)$$

Figs. 5 and 6 show the coefficient $c(\lambda, z)$ calculated using Eq. (8) with the two considered chlorophyll profiles, for different wind speeds and only for the most convenient wavelenght values, as identified from Figs. 2 and 3, i.e., 492.5 nm and 575 nm, corresponding to cyan and yellow light, respectively. As expected, the impact of bubbles only affects the first part of the propagation path, near the surface, and tends to become zero after about 5-10 meters.

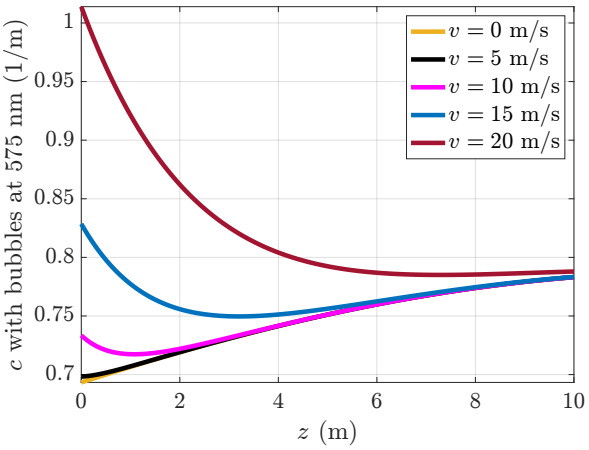

Fig. 6. Attenuation coefficient versus depth for surface concentration $C_\mathrm{s} = 2$ mg/m^3 and $\lambda = 575$ nm, including bubble contribution.

III. Power Losses in Vertical Links

Using the attenuation coefficient defined by Eq. (8), the loss affecting the signal as it propagates through the water can be calculated with the Beer-Lambert law. Results are reported in Figs. 7 and 8 for the two different surface chlorophyll values, for $v_{10} = 0$ m/s, that is by neglecting the effect of bubbles. We notice that for the highest value of C_s the loss becomes extremely large after just a few tens of meters. It is interesting to notice that, for the low C_s, there is a change in the slope of the loss curve versus depth. This means that the first segment of the water, closer to the surface, is the most critical one and, after about 50 meters, light propagation becomes much easier, being less affected by scattering. This is due to the peak in the chlorophyll concentration arising at relatively low depth.

Finally, Fig. 9 shows the effects of water bubbles on the losses. We limit the analysis to the case of $C_\mathrm{s} = 0.5$ mg/m^3 and cyan light at 492.5 nm, but similar conclusions can be drawn in other cases. The impact of bubbles causes a further loss of 1-3 dB, which is higher for stronger wind speed.

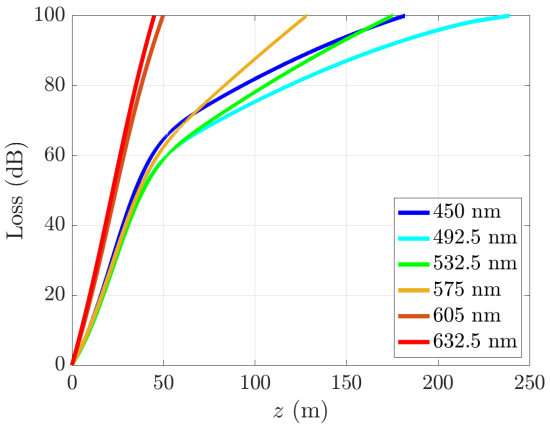

Fig. 7. Losses versus depth for surface concentration $C_s = 0.5$ mg/m^3 and different signal wavelengths.

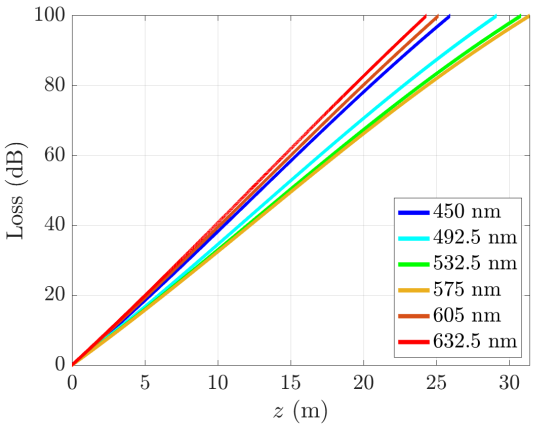

Fig. 8. Losses versus depth for surface concentration $C_s = 2$ mg/m^3 and different signal wavelengths.

IV. Conclusions

In this paper we analyzed the propagation of visible light in underwater vertical links, taking into account the main effects as a function of wavelength and depth. Attenuation coefficient and power loss have been computed for different water types, considering also the presence of water bubbles, with the aim of identifying the best transmission wavelength. The presented results demonstrate that blue, cyan and green present the lowest attenuation coefficient, while yellow light can represent an alternative in the first tens of meters beneath the surface, being less affected by scattering.

Future work will include the identification of the optimal range for wavelength division multiplexing with multiple visible light channels, in order to increase the throughput of the vertical underwater communication link. Another important aspect to consider is the evaluation of communication performance (e.g., in terms of error rate) using the developed realistic underwater channel model.

Acknowledgment

This work was supported by the European Space Agency under the framework of SatNEx V project. The view expressed herein can in no way be taken to reflect the official opinion of the European Space Agency.

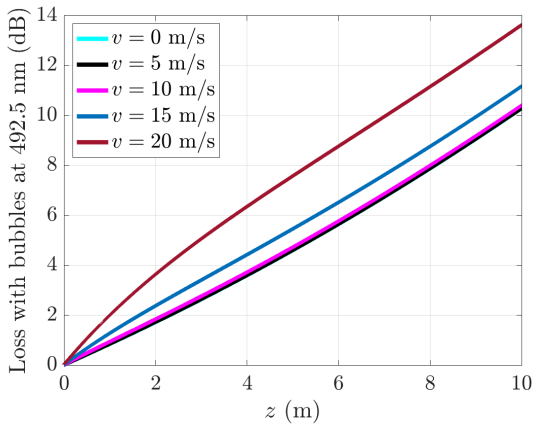

Fig. 9. Losses versus depth for surface concentration Cs = 0.5 mg/m3 and different signal wavelengths, including bubble contribution.

References

[1] H. Kaushal and G. Kaddoum, "Underwater optical wireless communication," *IEEE Access*, vol. 4, pp. 1518–1547, Apr. 2016.

[2] C. Gabriel, M.-A. Khalighi, S. Bourennane, P. Leon, and V. Rigaud, "Monte-carlo-based channel characterization for underwater optical communication systems," *IEEE/OSA J. Opt. Commun. Networking*, vol. 5, no. 1, pp. 1–12, 2013.

[3] V. I. Haltrin, "Chlorophyll-based model of seawater optical properties," *Appl. Opt.*, vol. 38, no. 33, pp. 6826–6832, Nov. 1999.

[4] T. Kameda and S. Matsumura, "Chlorophyll biomass off Sanriku, northwestern Pacific, estimated by ocean color and temperature scanner (OCTS) and a vertical distribution model." *J Oceanogr*, vol. 54, pp. 509–516, Sep. 1998.

[5] A. Ugolini, F. Poli, D. Croce, and S. Mangione, "Depth-dependent channel characterization for visible light in underwater optical wireless links," in *Proc. Intern. Symposium on Commun. Systems, Networks and Digital Signal Processing (CSNDSP)*, Rome, Italy, Jul. 2024.

[6] L. J. Johnson, R. J. Green, and M. S. Leeson, "Underwater optical wireless communications: depth dependent variations in attenuation," *Appl. Opt.*, vol. 52, no. 33, pp. 7867–7873, Nov. 2013.

[7] A. Bricaud, M. Babin, A. Morel, and H. Claustre, "Variability in the chlorophyll-specific absorption coefficients of natural phytoplankton: Analysis and parameterization," *J. of Geophysical Research: Oceans*, vol. 100, no. C7, pp. 13 321–13 332, 1995.

[8] R. M. Pope and E. S. Fry, "Absorption spectrum (380–700 nm) of pure water. II. Integrating cavity measurements," *Appl. Opt.*, vol. 36, no. 33, pp. 8710–8723, Nov. 1997.

[9] J. Hong, J. Zou, Y. Wang, Q. Ruan, T. Chen, Y. Cheng, Y. Bu, and Z. Luo, "All-fiber cyan laser at 491.5 nm," *Opt. Lett.*, vol. 48, no. 5, pp. 1327–1330, Mar. 2023.

[10] M.-P. Lord, L. Talbot, M. Bernier, and R. Vallée, "Monolithic silica fiber laser operating at 585 nm," *Opt. Lett.*, vol. 48, no. 2, pp. 514–517, Jan. 2023.

[11] J. Zou, J. Hong, Z. Zhao, Q. Li, Q. Ruan, H. Wang, Y. Bu, X. Guan, M. Zhou, Z. Feng, and Z. Luo, "3.6 W compact all-fiber Pr^{3+}-doped green laser at 521 nm," *Adv. Photonics*, vol. 4, no. 5, p. 056001, 2022.

[12] R. S. Keiffer, J. C. Novarini, and G. V. Norton, "The impact of the background bubble layer on reverberation-derived scattering strengths in the low to moderate frequency range," *J. Acoust. Soc. Am.*, vol. 97, no. 1, pp. 227–234, Jan. 1995.